Soft Matter

PAPER

View Article Online
View Journal | View Issue

Cite this: *Soft Matter*, 2016, 12, 9297

Received 5th August 2016,
Accepted 31st October 2016

DOI: 10.1039/c6sm01804a

www.rsc.org/softmatter

Assembly of diverse molecular aggregates with a single, substrate-directed molecule orientation†

Frank Balzer,*[a] Matthias Schulz,[b] Arne Lützen[b] and Manuela Schiek[c]

Oriented, fluorescing organic nanoaggregates derived from 1,4‴-dicyano-functionalized *para*-quaterphenylene (CNP4) are obtained upon vacuum deposition on muscovite mica. Two types of aggregates are observed with fiber- and wing-like shape, respectively, both growing along distinct substrate directions. The polarization of the emitted fluorescence, their morphology, and their electric surface potential differ, reflecting different polymorphs. The wings are chiral twins. The molecules orient within ±5° along the same direction, templated by the substrate.

1 Introduction

Small conjugated organic molecules crystallizing into low-dimensional assemblies by physical vapor deposition, template assisted wetting of porous substrates, or by self-assembly in solution phase have attracted considerable interest for a widespread number of uses such as, *e.g.*, templates for electrochemical applications[1–5] or photovoltaics.[6] Self-organization into either parallel or perpendicular to the substrate surface oriented assemblies[7–9] including chiral organization[10] is of special advantage for optical purposes such as waveguiding,[11] exciton–polariton coupling,[12,13] frequency doubling,[14] and lasing.[15,16] Functionalization together with epitaxy is used to control optical and morphological properties of the assemblies.[17–19] In this context, cyano-functionalization is of special interest due to the asymmetric charge distribution and the electron-withdrawing effect.[20,21] Cyano groups are capable of forming hydrogen bonds in the solid state, impacting molecular packing and thin film formation,[22] and consequently optical properties, *e.g.* enhancement of fluorescence quantum yields.[23] The effect of the cyano groups on the crystal structure is, *e.g.*, reported for thiophene/phenylene co-oligomers and squaraines.[24,25]

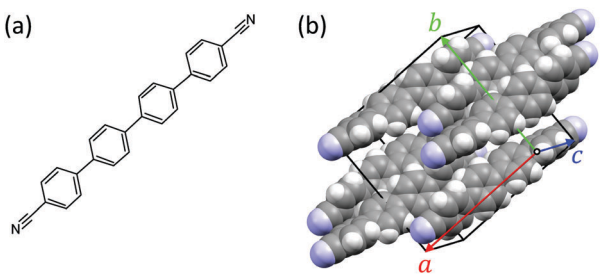

Fig. 1 (a) Structural formula of the cyano-functionalized *para*-quaterphenylene CNP4. (b) In the bulk the molecules crystallize into a monoclinic unit cell (solid lines).[26]

Here, the formation of discontinuous thin films of the prototypical, 1,4‴-dicyano-functionalized *para*-quaterphenylene (CNP4) is investigated, together with their optical and electrical properties. The molecules are vacuum deposited on muscovite mica. The structural formula of CNP4 and the bulk crystal structure[26] are shown in Fig. 1. The molecule crystallizes into a monoclinic unit cell (space group $C2/c$) with four molecules and lattice constants a = 16.337(3) Å, b = 16.855(3) Å, c = 7.4845(15) Å, and β = 112.68(3)°. Each molecule is not planar but exhibits a screw-like structure.[27]

Muscovite mica has already served as a model substrate for studies on organic nanofibers. It is mechanically flexible, optically transparent in the visible wavelength region, and its cleavability along the (001) planes allows the creation of macroscopic, atomically flat surfaces.[28] It supports – sometimes after the formation of a wetting layer[29,30] – three-dimensional, epitaxial growth of organic molecules. Due to its *cm* surface symmetry, this growth is highly anisotropic[31–33] as also observed for other anisotropic surfaces such as TiO_2(110)[34,35] and Cu(110).[36,37] On the muscovite (001) face, the mirror plane changes from along [110] to [$\bar{1}$10] and back at consecutive cleavage planes.[29,38,39] The anisotropy

[a] *NanoSyd, Mads Clausen Institute, University of Southern Denmark, DK-6400 Sønderborg, Denmark. E-mail: fbalzer@mci.sdu.dk; Tel: +45 6550 1655*
[b] *Kekulé Institute of Organic Chemistry and Biochemistry, Rheinische-Friedrich-Wilhelms-University of Bonn, Gerhard-Domagk-Str. 1, D-53121 Bonn, Germany*
[c] *Energy and Semiconductor Research Laboratory, Institute of Physics, University of Oldenburg, Carl-von-Ossietzky-Str. 9-11, D-26129 Oldenburg, Germany*

† Electronic supplementary information (ESI) available: AFM images and XRD patterns (Fig. S1, S2, S6, S7, and S8), distribution analysis and correlation plots (Fig. S4 and S5), fluorescence spectra (Fig. S3). AFM-movie of aging (CNP4_aging.avi). See DOI: 10.1039/c6sm01804a

changes accordingly, leading to two rotational nanofiber domains. After formation, fibers can be wet-transferred to a substrate of choice for further processing.[7]

2 Experimental

The synthesis of 1,4‴-dicyano-4,1′:4′,1″:4″,1‴-quaterphenylene (CNP4) has been described earlier.[40] Briefly, the synthesis was achieved in a twofold Suzuki cross-coupling reaction from 4-cyano phenyl boronic acid and 4,4′-dibromobiphenyl. The CNP4 precipitate was collected by filtration and purified by washing with solvents, resulting in the final, highly pure compound. At a substrate temperature T_s, the molecules are deposited by thermal sublimation in high vacuum (base pressure 1×10^{-8} mbar) onto freshly cleaved muscovite mica (grade V-4, Structure Probe, Inc.).[29] All given temperatures are sample holder temperatures. *Ex situ*, the sample morphology and electric surface potential are investigated by atomic force microscopy in intermittent contact mode with a highly doped Si tip (AFM, JPK NanoWizard, NanoWorld Pointprobe NCH tip), and by Kelvin probe force microscopy (KPFM) using hover mode (lift height 50 nm) with either the same NCH tip or with a Cr/Pt coated Si tip (BudgetSensors Tap 300E-G). For fluorescence microscope images a Nikon Eclipse ME-600 epifluorescence microscope with a high-pressure mercury lamp (excitation wavelength $\lambda_{exc} \approx 365$ nm) and appropriate cut-off filters is used. The polarization of the emitted fluorescence light is resolved spatially with a linear polarizer in front of the microscope camera (PixeLINK PL-B873-CU) and by a computer-controlled rotation (Thorlabs PRM1Z8) of the sample.[33] This in-plane rotation is conducted over 360° in steps of 5°. From a discrete Fourier analysis of the angle dependent fluorescence intensity, the angle of maximum fluorescence ϕ_{pol} is determined for each pixel.[41,42] Assuming that the transition dipole between the excited state S_1 and the ground state S_0 of CNP4 is parallel to its long molecule axis,[33,43,44] ϕ_{pol} reflects the averaged orientation of the long molecule axes for this image pixel. This direction is related to the muscovite high symmetry directions [100], [110], and [$\bar{1}$10], which are determined by means of a percussion figure.[45,46] Because the SiO_4 tetrahedra on the muscovite (001) face are tilted, one of the two ⟨110⟩ directions is grooved. This direction is denoted in the following by the index "g".[47,48] The non-grooved ⟨110⟩ direction is marked by the index "ng". X-ray diffraction is performed in the Bragg–Brentano configuration with a PANalytical X'PertPro MPD diffractometer (Cu-K_α radiation, automatic divergence slit).

3 Results and discussion

The vacuum deposition of CNP4 onto muscovite mica leads to the formation of elongated nanoaggregates,[49] as demonstrated in Fig. 2 and 3. Within a single substrate domain, these aggregates roughly show three growth directions. Two different domains exist on a single sample, mutually rotated by 120°. The three growth directions are not equivalent. Besides mutually aligned fibers with a triangular cross-section, growing within

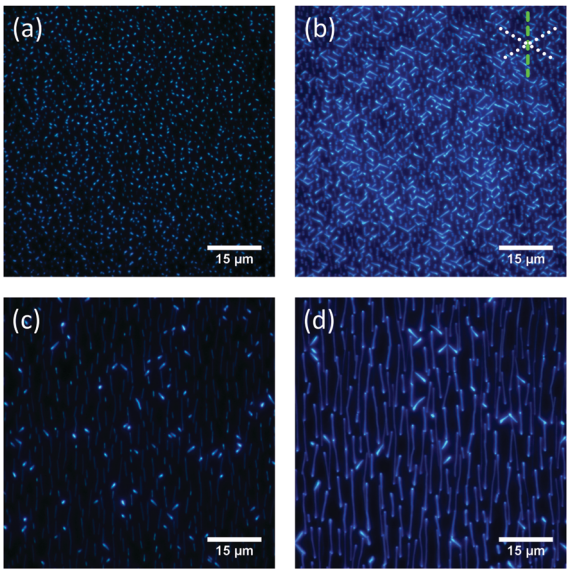

Fig. 2 Fluorescence microscope images of CNP4 aggregates grown on muscovite mica at different deposition temperatures T_s and with different nominal thicknesses d. (a) and (b): T_s = 313 K with d = 2 nm and d = 10 nm, respectively. (c) and (d): T_s = 343 K with the same nominal thicknesses as in (a) and (b). The dashed green line in (b) depicts the grooved muscovite direction $\langle 110 \rangle_g$, the dotted white lines [100] and $\langle 110 \rangle_{ng}$.

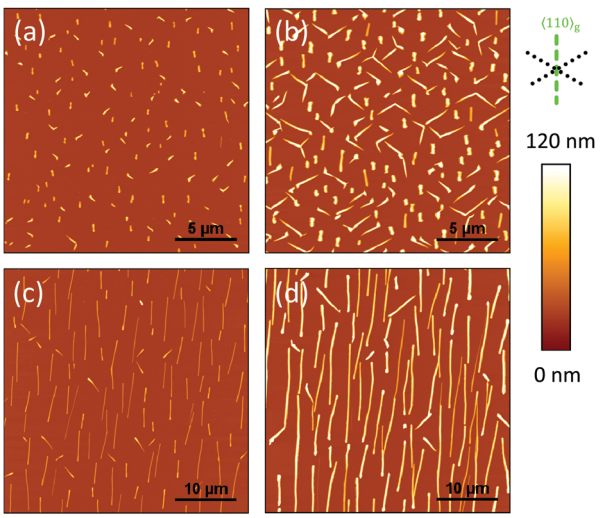

Fig. 3 Corresponding AFM images of the CNP4 aggregates presented in Fig. 2. Muscovite high-symmetry directions are denoted in the upper right.

±10° along $\langle 110 \rangle_g$, a second type of assemblies with increased heights is visible. Their triangular shape is often less well defined and reminds of wings. They grow approximately along the other two muscovite high-symmetry directions, their fluorescence being stronger than that of the fibers. No epitaxial wetting layer has been detected by low energy electron diffraction (LEED).[10,29,50]

According to Fig. 2 and 3, for a substrate temperature of T_s = 343 K and for a nominal film thickness of 10 nm, the fibers possess a mean length of about 10 µm. Their typical width is several 100 nm, and heights up to 100 nm are found. A single wing exhibits a mean length of approximately 5 µm with a

similar width as the fiber-like structures. Note that whereas the height of a single fiber is uniform, the height of a single wing often increases by a factor of two from one end to the other. This larger amount of material might be at least partly responsible for the stronger fluorescence of the wings.

The samples show some aging under ambient conditions: wings are growing at the expense of fibers, Fig. S1 and Movie S1 (ESI†).[51] Directly after vacuum deposition, often clusters are observed between the fibers. This is shown in Fig. S1 and S2(a) (ESI†) and has been reported previously for the case of other *para*-phenylenes, thiophenes, and naphthyl end-capped thiophenes.[10,19,50] The clusters tend to vanish on the timescale of days under ambient conditions due to Ostwald ripening. As long as the aggregates are not too small, the overall morphological appearance of the samples stored under ambient conditions as well as their fluorescence properties are stable over the span of at least 9×10^4 hours.

After illumination with UV light, the aggregates emit polarized blue fluorescence light; a spectrum is given in Fig. S3 (ESI†). For an isolated *para*-phenylene molecule, its polarization is parallel to the long molecule axis.[43,44] Since the molecule orientation also determines the optical indicatrix and polarization properties of fibers and wings,[33,52] a spatially resolved polarization analysis reveals the projection of the long molecule axis onto the substrate surface. From the orientation of the long fiber or wing axis, θ_{orient}, the angle of the long molecule axis with respect to the long aggregate axis is calculated, $\beta_{mol} = \phi_{pol} - \theta_{orient}$. An angle of $\beta_{mol} = 90^\circ$ means, that the emitted light is polarized perpendicular to the long aggregate axis; for $\beta_{mol} = 0^\circ$ and 180° it is polarized parallel to it.

On a global scale, Fig. 4(a), Fig. S4(a) and S5(a) (ESI†), three growth directions are identified (solid black line). The fibers growing along the grooved muscovite direction show an angular distribution of $\pm 10^\circ$. The wings do not grow exactly along the other high-symmetry directions $\langle 110\rangle_{ng}$ and [100]. In general, a rather large range of angles with respect to $\langle 110\rangle_g$ between $\pm 30(5)^\circ$ and $\pm 70(5)^\circ$ is observed. The emitted light is, however, for all of the observed growth directions within $\pm 10^\circ$ polarized perpendicular to the grooved mica direction, see the dashed red line in Fig. 4(a). Here, the wings include angles of $\pm 35(5)^\circ$ with respect to $\langle 110\rangle_g$. The distribution of molecule orientations within the aggregates peaks at three different values: $\beta_{mol} = 90^\circ$, 50°, and 40°, Fig. 4(b), and at their mirrors at $180^\circ - \beta_{mol}$.

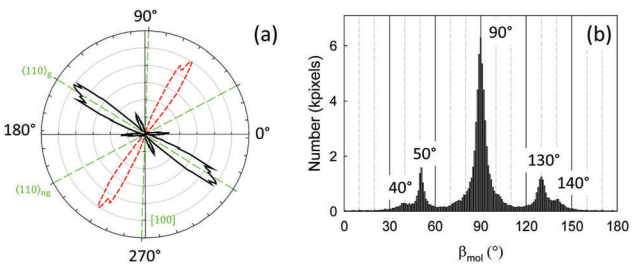

Fig. 4 (a) Orientational (solid black line) and polarization (dashed red line) analysis of a typical CNP4 sample grown on muscovite mica. Three different values for β_{mol} are preferred by the aggregates, (b). The fluorescence microscope image is shown in Fig. 5(a).

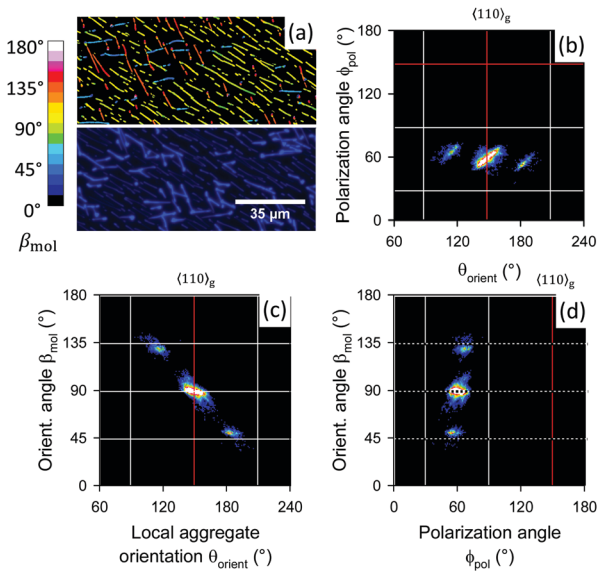

Fig. 5 The lower part of (a) shows an unpolarized fluorescence microscope image of CNP4 aggregates; in the upper part the orientational angle β_{mol} is superimposed. Correlation plots (b)–(d) demonstrate the relations between the different quantities from Fig. 4. Solid white lines mark muscovite high-symmetry directions, red lines $\langle 110\rangle_g$.

Since three different aggregate orientations with similar polarization properties are observed, the molecule orientations within have to be correlated. This is already shown in the upper part of Fig. 5(a): specific aggregate directions correspond to distinct values of β_{mol}. Correlation plots confirm these observations. The polarization angle ϕ_{pol} is within $\pm 10^\circ$ independent from the local aggregate orientation, Fig. 5(b). A correlation plot of the local fiber orientation θ_{orient} and of the orientational angle β_{mol}, Fig. 5(c), shows that the optical properties of the wings are different from that of the fibers. For the fibers β_{mol} is $90(10)^\circ$, *i.e.*, the long molecule axis is perpendicular to the local long fiber axis, whereas for the wings two values are observed, $50(5)^\circ$ and $40(5)^\circ$. Since the angle between the fibers and wings can vary between $\pm 35^\circ$ and $\pm 70^\circ$, depending on, *e.g.*, deposition temperature, also β_{mol} varies accordingly, Fig. S4 and S5 (ESI†). The polarization angle ϕ_{pol}, however, is always within $\pm 10^\circ \perp \langle 110\rangle_g$, Fig. 5(d). The molecule orientations within the two wing directions are not identical, but differ consistently by $\pm 5^\circ$ with respect to the fibers. Such a behavior, where the substrate induces a small range of molecule orientations, but different aggregate orientations, is rather unusual. It has not been reported for other functionalized *para*-quaterphenylenes, yet.

Opposite to the formation of aligned fibers on muscovite, the vacuum deposition of CNP4 on glass leads to the disordered growth of short fibers and crystallites, see Fig. S6(a) (ESI†). At higher deposition temperatures the crystallites become taller, but more separated. This Frank–van der Merwe growth is in opposite to, *e.g.*, the epitaxial growth of a *para*-quaterphenylene functionalized with electron-donating methoxy groups,[53] where islands and layers from upright standing molecules form.[54]

Contact planes and *d*-spacings of the films are determined by X-ray diffraction; diffractograms for CNP4 deposited on

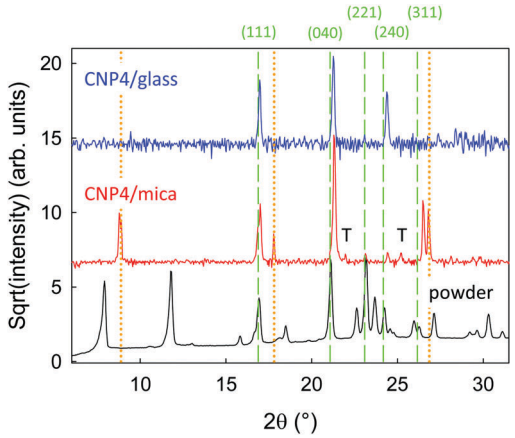

Fig. 6 X-ray diffractograms of CNP4 powder (black line), CNP4 deposited on glass (upper blue line), and on muscovite mica with subsequent wet transfer to glass (middle red line). Vertical dashed green lines mark the positions of some of the bulk reflections. The "T" denote weak reflections which cannot be related to the bulk structure. Dotted orange vertical lines finally mark strong reflections from muscovite mica. For the CNP4 films the glass background has been subtracted.

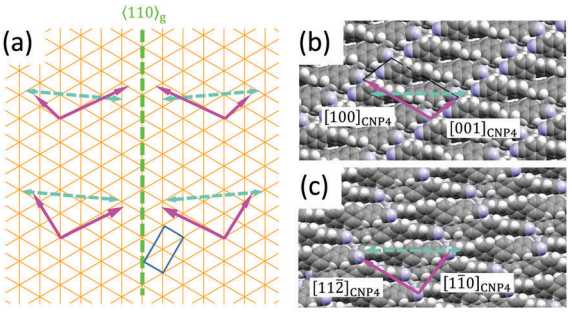

Fig. 7 (a) Possible alignment of the CNP4 (040) and (111) faces on the hexagonal muscovite mica lattice (orange solid lines), forming wings. The muscovite $\langle 110\rangle_g$ direction is emphasized by a vertical green, dashed line, its surface unit cell by a solid blue line. Pink solid arrows mark the unit cells of the two CNP4 faces shown in (b) and (c) together with their mirrored counterparts, the dashed cyan lines denote the long molecule axes. In (b) the arrangement of CNP4 molecules on the (040) face is shown, in (c) for the (111) face. Proposed aggregate directions are along the short unit cell axes.

muscovite, for CNP4 powder, and for CNP4 deposited on glass are shown in Fig. 6. For a comparison with a calculated diffractogram derived from the bulk crystal structure see Fig. S6(b) (ESI†). For this characterization technique, the amount of deposited organic material has to be considerably larger than for, *e.g.*, the optical or morphological investigations. AFM images of a nominally 60 nm thick sample, Fig. S7 (ESI†), show a similar morphology than observed for a few nanometer thin samples, except that fibers and wings are taller and wider. To get rid of strong diffraction peaks from the muscovite substrate, which might overlap with ones from CNP4, Fig. S8 (ESI†), the CNP4 aggregates often have been wet-transferred to glass prior to their XRD characterization.[55] By control experiments it has been assured that the same diffraction peaks are observed for fibers and wings still remaining on the mother substrate, so that the wet transfer does not significantly change the contact planes. Most of the observed diffraction peaks can be assigned to the bulk structure. For CNP4 deposited on glass, the (111), (040), and (240) faces are observed to be parallel to the substrate. All those correspond to lying molecules. Most peaks are slightly shifted to larger diffraction angles compared to the measured counterparts from CNP4 powder, resulting from a slightly shortened *d*-spacing by approximately 0.04 Å. This slightly more dense packing of the molecules is probably due to a surface-induced modification of the crystal phase. A similar trend is observed for CNP4 on muscovite. Opposite to the deposition on glass, additional diffraction peaks with varying intensities are observed, which cannot be assigned to the bulk, Fig. S8 (ESI†). They are marked by a "T". Diffraction from mica is still visible, probably from wet-transferred mica flakes. Their positions are marked by vertical, dotted orange lines.

In the bulk structure of CNP4 the molecules are packed in rows along the CNP4 [001] direction,[26] as depicted in Fig. 1(b). Due to the oblique angle of the molecules long axes with the CNP4 [001] direction and due to the arrangement of the molecules in the unit cell, it is not straightforward to assign a possible fiber direction for a given contact face as for the case of, *e.g.*, *para*-hexaphenylene.[29] The optical polarization properties of the wings can be reproduced with some of the observed bulk crystal faces. For, *e.g.*, the identified (040) contact plane, the angle of the long molecule axis with respect to the fiber axis is probably 37°, as shown in Fig. 7(b), assuming that in this case the fiber direction is along CNP4 [001]. Assuming further on, that the long molecule axis is either at 5° or −5° perpendicular to $\langle 110\rangle_g$, the fiber direction is about 47° off from $\langle 110\rangle_g$. For the CNP4 (111) face, Fig. 7(c), an assumed aggregate growth direction along CNP4 $[1\bar{1}0]$ leads to aggregates 32° off, which agrees satisfactorily with the measured angle of 35(5)°. For the identified contact planes (240), (040), (111), and (311) values for β_{mol} between 30° and 37° are estimated, which can explain other observed wing directions. Similar to the growth of the methoxy-functionalized *para*-quaterphenylene MOP4, the two wings resemble twins with a chiral organization into single-handed aggregates, induced by the substrate surface.[10] For any of the observed bulk contact planes, CNP4 high-symmetry directions and close packed faces seem not to be compatible with an orientational angle β_{mol} close to 90°. Therefore, we suggest that the fibers are formed by a surface induced phase.[56] The two orientations along $\langle 110\rangle_g$ then also resemble chiral twins. Under ambient conditions in contact with water vapor, the fibers are prone to aging and faceting,[57] the latter one especially during wet-transfer, Fig. S2(b) and S1 (ESI†). Both suggest a less stable crystal phase of the fibers in contact with water.

To characterize the electrostatic properties of the samples, KPFM is a powerful tool to obtain high-resolution maps of the contact potential difference (CPD).[58–60] The mapping of the CPD for CNP4 aggregates is demonstrated in Fig. 8. In Fig. 8(a) the topography of a CNP4 sample of fibers and wings is shown. The electrical properties are shown in Fig. 8(b). A clear contrast is observed between the muscovite substrate on one hand, and the two different aggregate types on the other hand: The fibers exhibit an up to 50 meV more positive surface potential than muscovite, the taller wings an 100 meV more negative surface potential.

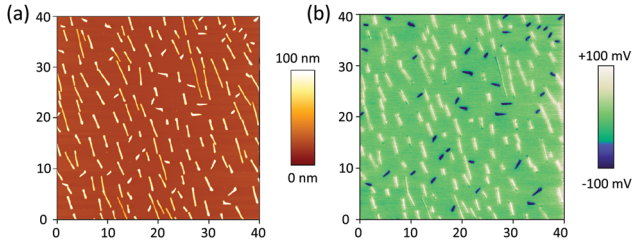

Fig. 8 AFM microscopy (a) and Kelvin probe force microscopy (b) of CNP4 aggregates. The KPFM image has been leveled to the muscovite surface potential.

These results suggest, that the wings either obtain a positive charge, or a dipole moment pointing out of the substrate surface, whereas it is opposite for the fibers.[61] This strong difference supports the assumption of different crystallographic contact faces for fibers and wings, as already discussed above. The size of the shift is comparable to other organic nanofibers. For, *e.g.*, nanofibers from a methoxy-functionalized *para*-quaterphenylene grown on muscovite mica, also a negative shift of 100 meV has been observed.[62]

4 Conclusions

A clear preference of the CNP4 molecules to adsorb flat lying with their long molecule axis within $\pm 10^{\circ}$ perpendicular to the muscovite mica $\langle 110 \rangle_g$ direction has been observed. However, still a number of growth directions are realized. This growth behavior is different from other fiber forming molecules on muscovite, where usually a single molecule orientation either leads to aggregates which are aligned parallel to each other, or where different fiber orientations are realized due to different preferred molecule orientations on the substrate. Here, the quasi parallel alignment of the molecules within all aggregates of different contact planes is probably due to the strong electron-withdrawing cyano groups. Electrostatic interactions dictate the growth, not necessarily epitaxy. Still, an epitaxial metric can be used to predict the growth by, *e.g.*, point-on-line or line-on-line epitaxy[10,63] and in fact often reproduces the right aggregate orientation for the observed contact planes. For a quantitative model though the epitaxial relationships and contact planes for individual aggregates have to be obtained by, *e.g.*, single area electron diffraction or by the X-ray pole figure technique.[64,65]

Acknowledgements

AL thanks the German research foundation DFG for financial support.

References

1 M. K. Debe and R. Poirier, *J. Vac. Sci. Technol., A*, 1994, **12**, 2017–2022.
2 D. F. van der Vliet, C. Wang, D. Tripkovic, D. Strmcnik, X. F. Zhang, M. K. Debe, R. T. Atanasoski, N. M. Markovic and V. R. Stamenkovic, *Nat. Mater.*, 2012, **11**, 1051–1058.
3 S. K. Saikin, A. Eisfeld, S. Valleau and A. Aspuru-Guzik, *Nanophotonics*, 2013, **2**, 21–38.
4 K. Bordo, M. Schiek and H.-G. Rubahn, *Appl. Phys. A: Mater. Sci. Process.*, 2014, **114**, 1067–1074.
5 S. Chen, P. Slattum, C. Wang and L. Zang, *Chem. Rev.*, 2015, **115**, 11967–11998.
6 F. Kim, G. Ren and S. Jenekhe, *Chem. Mater.*, 2011, **23**, 682–732.
7 M. Schiek, F. Balzer, K. Al-Shamery, J. Brewer, A. Lützen and H.-G. Rubahn, *Small*, 2008, **4**, 176–181.
8 L. Jiang, H. Dong and W. Hu, *Soft Matter*, 2011, **7**, 1615–1630.
9 Z. Ma, Z. Hu, H. Zhang, M. Peng, X. He, Y. Li, Z. Yang and J. Qiu, *J. Mater. Chem. C*, 2016, **4**, 1029–1038.
10 F. Balzer, C. Röthel, H.-G. Rubahn, A. Lützen, J. Parisi, R. Resel and M. Schiek, *J. Phys. Chem. C*, 2016, **120**, 7653–7661.
11 F. Balzer, V. Bordo, A. Simonsen and H.-G. Rubahn, *Phys. Rev. B: Condens. Matter Mater. Phys.*, 2003, **67**, 115408.
12 B. Rogez, R. Horeis, E. L. Moal, J. Christoffers, K. Al-Shamery, G. Dujardin and E. Boer-Duchemin, *J. Phys. Chem. C*, 2015, **119**, 22217–22224.
13 R. Chikkaraddy, P. P. Patra, R. P. N. Tripathi, A. Dasgupta and G. P. Kumar, *Nanoscale*, 2016, **8**, 14803–14808.
14 K. Pedersen, M. Schiek, J. Rafaelsen and H.-G. Rubahn, *Appl. Phys. B: Lasers Opt.*, 2009, **96**, 821–826.
15 F. Quochi, F. Cordella, A. Mura, G. Bongiovanni, F. Balzer and H.-G. Rubahn, *Appl. Phys. Lett.*, 2006, **88**, 041106.
16 J. Gierschner, S. Varghese and S. Y. Park, *Adv. Opt. Mater.*, 2016, **4**, 348–364.
17 M. Schiek, A. Lützen, K. Al-Shamery, F. Balzer and H.-G. Rubahn, *Cryst. Growth Des.*, 2007, **7**, 229–233.
18 R. Resel, T. Haber, O. Lengyel, H. Sitter, F. Balzer and H.-G. Rubahn, *Surf. Interface Anal.*, 2009, **41**, 764–770.
19 F. Balzer, M. Schiek, A. Osadnik, I. Wallmann, J. Parisi, H.-G. Rubahn and A. Lützen, *Phys. Chem. Chem. Phys.*, 2014, **16**, 5747–5754.
20 P. A. Wood, S. J. Borwick, D. J. Watkin, W. D. S. Motherwell and F. H. Allen, *Acta Crystallogr., Sect. B: Struct. Sci.*, 2008, **64**, 393–396.
21 S. Gottardi, K. Müller, J. C. Moreno-López, H. Yildirim, U. Meinhardt, M. Kivala, A. Kara and M. Stöhr, *Adv. Mater. Interfaces*, 2013, **1**, 1300025.
22 F. Klappenberger, *Prog. Surf. Sci.*, 2014, **89**, 1–55.
23 C. Li, M. Hanif, X. Li, S. Zhang, Z. Xie, L. Liu, B. Yang, S. Su and Y. Ma, *J. Mater. Chem. C*, 2016, **4**, 7478–7484.
24 H. Yanagi, H. Mizuno, F. Sasaki and S. Hotta, in *Chemical Science of π-Electron Systems*, Springer, 2015, ch. 38, pp. 635-654.
25 D. Yang, Y. Jiao, L. Yang, Y. Chen, S. Mizoi, Y. Huang, X. Pu, Z. Lu, H. Sasabe and J. Kido, *J. Mater. Chem. A*, 2015, **3**, 17704–17712.
26 F. Klappenberger, D. Kühne, M. Marschall, S. Neppl, W. Krenner, A. Nefedov, T. Strunskus, K. Fink, C. Wöll, S. Klyatskaya, O. Fuhr, M. Ruben and J. Barth, *Adv. Funct. Mater.*, 2011, **21**, 1631–1642.
27 A. Moser, O. Werzer, H.-G. Flesch, M. Koini, D.-M. Smilgies, D. Nabok, P. Puschnig, C. Ambrosch-Draxl, M. Schiek,

H.-G. Rubahn and R. Resel, *Eur. Phys. J.: Spec. Top.*, 2009, **167**, 59–65.
28 C. Simbrunner, *Semicond. Sci. Technol.*, 2013, **28**, 053001.
29 F. Balzer and H.-G. Rubahn, *Surf. Sci.*, 2004, **548**, 170–182.
30 P. Frank, G. Hlawacek, O. Lengyel, A. Satka, C. Teichert, R. Resel and A. Winkler, *Surf. Sci.*, 2007, **601**, 2152–2160.
31 N. Uyeda, M. Ashida and E. Suito, *J. Appl. Phys.*, 1965, **36**, 1453–1460.
32 S. Kobzareva and G. Distler, *J. Cryst. Growth*, 1971, **10**, 269–275.
33 F. Balzer and M. Schiek, in *Bottom-Up Self-Organization in Supramolecular Soft Matter*, ed. S. C. Müller and J. Parisi, Springer, Berlin, 2015, vol. 217, ch. 7, pp. 151–176.
34 G. Koller, S. Berkebile, J. Krenn, G. Tzvetkov, G. Hlawacek, O. Lengyel, F. Netzer, C. Teichert, R. Resel and M. Ramsey, *Adv. Mater.*, 2004, **16**, 2159–2162.
35 D. Wrana, M. Kratzer, K. Szajna, M. Nikiel, B. R. Jany, M. Korzekwa, C. Teichert and F. Krok, *J. Phys. Chem. C*, 2015, **119**, 17004–17015.
36 T. Djuric, T. Ules, H.-G. Flesch, H. Plank, Q. Shen, C. Teichert, R. Resel and M. Ramsey, *Cryst. Growth Des.*, 2011, **11**, 1015–1020.
37 J. Novák, M. Oehzelt, S. Berkebile, M. Koini, T. Ules, G. Koller, T. Haber, R. Resel and M. G. Ramsey, *Phys. Chem. Chem. Phys.*, 2011, **13**, 14675.
38 E. Suito, N. Uyeda, M. Ashida and K. Yamamoto, *Proc. Jpn. Acad.*, 1966, **42**, 54–59.
39 G. Distler, E. Kortukova and S. Kobzareva, *Krist. Tech.*, 1973, **8**, 67–75.
40 M. Schiek, K. Al-Shamery and A. Lützen, *Synthesis*, 2007, 613–621.
41 U. Bernchou, J. Brewer, H. Midtiby, J. Ipsen, L. Bagatolli and A. Simonsen, *J. Am. Chem. Soc.*, 2009, **131**, 14130–14131.
42 K. Bordo, M. Schiek, A. Ghazal, I. Wallmann, A. Lützen, F. Balzer and H.-G. Rubahn, *J. Phys. Chem. C*, 2011, **115**, 20882–20887.
43 I. B. Berlman, H. O. Wirth and O. J. Steingraber, *J. Phys. Chem.*, 1971, **75**, 318–325.
44 N. Nijegorodov, W. Downey and M. Danailov, *Spectrochim. Acta, Part A*, 2000, **56**, 783–795.
45 C. Frondel and G. Ashby, *Am. Mineral.*, 1937, **22**, 104–121.
46 R. Jahns and F. Lancaster, *Physical Characteristics of Commercial Sheet Muscovite in the Southeastern United States*, United States Government Printing Office Geological Survey Professional Paper 225, 1950.
47 Y. Kuwahara, *Phys. Chem. Miner.*, 1999, **26**, 198–205.
48 Y. Kuwahara, *Phys. Chem. Miner.*, 2001, **28**, 1–8.
49 M. Schiek, F. Balzer, K. Al-Shamery, A. Lützen and H.-G. Rubahn, *Soft Matter*, 2008, **4**, 277–285.
50 A. Winkler, *Surf. Sci.*, 2016, **643**, 124–137.
51 I. Horcas, R. Fernandez, J. Gomez-Rodriguez, J. Colchero, J. Gomez-Herrero and A. Baro, *Rev. Sci. Instrum.*, 2007, **78**, 013705.
52 P. Fesenko, C. Rolin, R. Janneck, S. P. Bommanaboyena, H. Gaethje, P. Heremans and J. Genoe, *Org. Electron.*, 2016, **37**, 100–107.
53 S. Takenaka, Y. Sakurai, H. Takeda, T. Ikemoto, H. Miyake, S. Kusabayashi and T. Takagi, *Mol. Cryst. Liq. Cryst.*, 1990, **178**, 103–115.
54 F. Balzer, R. Sun, J. Parisi, H.-G. Rubahn, A. Lützen and M. Schiek, *Thin Solid Films*, 2015, **597**, 104–111.
55 J. Brewer, H. Henrichsen, F. Balzer, L. Bagatolli, A. Simonsen and H.-G. Rubahn, *Proc. SPIE*, 2005, **5931**, 59310Y.
56 A. O. F. Jones, B. Chattopadhyay, Y. H. Geerts and R. Resel, *Adv. Funct. Mater.*, 2016, **26**, 2233–2255.
57 N. Zhang, L. Bu, S. Guo, J. Guo and X. Huang, *Nano Lett.*, 2016, **16**, 5037–5043.
58 V. Palermo, M. Palma and P. Samori, *Adv. Mater.*, 2006, **18**, 145–164.
59 T. Glatzel, L. Zimmerli, S. Koch, S. Kawai and E. Meyer, *Appl. Phys. Lett.*, 2009, **94**, 063303.
60 L. Nony, *Principles of Kelvin Probe Force Microscopy and applications*, 2013, 1st German-French Summer School on noncontact-AFM Porquerolles, https://cel.archives-ouvertes.fr/cel-00917935.
61 A. Hinaut, A. Pujol, F. Chaumeton, D. Martrou, A. Gourdon and S. Gauthier, *Beilstein J. Nanotechnol.*, 2012, **3**, 221–229.
62 F. Balzer, R. Sun, H.-G. Rubahn, M. Schiek and A. Lützen, *Proc. SPIE*, 2014, **8983**, 89830M.
63 D.-M. Smilgies and E. Kintzel, Jr., *Phys. Rev. B: Condens. Matter Mater. Phys.*, 2009, **79**, 235413.
64 R. Resel, *J. Phys.: Condens. Matter*, 2008, **20**, 184009.
65 T. Haber and R. Resel, in *Organic Nanostructures for Next Generation Devices*, ed. K. Al-Shamery, H.-G. Rubahn and H. Sitter, Springer, Berlin, 2008, vol. 101, pp. 119–165.